Text S1

We use the following multivariate predictive model (e.g., Stern and Kaufmann 2013, Mosedale *et al* 2006) to estimate the causal links between the ENSO and ozone concentration:

$$\boldsymbol{X_t = \sum_{i=1}^{p} \alpha_i X_{t-i} + \sum_{i=1}^{p} \beta_i Y_{t-i} + \sum_{j=1}^{m} \sum_{i=1}^{p} \delta_{j,i} Z_{j,t-i} + \varepsilon_t} \quad \textbf{(1)}$$

where X_t is the annual mean (or seasonal mean) ozone concentration for year t, Y_t is the ENSO index, and $Z_{j,t}$ is the confounding factor j for year t. In the predictive model shown in equation 1, while estimating the influence of Y on X (i.e., the contribution of the term $\sum_{i=1}^{p} \beta_i Y_{t-i}$ in predicting X), the contribution of past X events are already taken into account by adding the term $\sum_{i=1}^{p} \alpha_i X_{t-i}$. Thus, the causal influence of Y on X, if detected, is robust and the contribution of past X events are already considered in our analyses. Here, m is number of confounding factors and $p \geq 1$ is the order of the multivariate predictive model. The optimal order p is computed by minimizing the Schwarz criterion or the Bayesian information criterion (Schwarz 1978). The optimal orders might be different for each model.

The ENSO index was computed as the average sea surface temperature (SST) anomalies in the Niño 3.4 area (120–170°W; 5°N–5°S) in boreal winter (December–January–February, DJF). Confounding factors (i.e., the dipole mode index (DMI; Saji et al., 1999), the Southern Annular Mode (SAM) and the North Atlantic Oscillation (NAO; e.g., Hurrell et al., 2003)) may have effects on the connections between ENSO and ozone concentration. The DMI was given as the difference in boreal fall (September–October–November, SON) SST anomalies between two Indian Ocean regions of the western pole (50–70°E; 10°N–10°S) and southeastern pole (90–110°E; 0°N–10°S). The SAM (Cai et al., 2011) was calculated as the first empirical orthogonal function (EOF) of the boreal summer (June–July–August, JJA) sea level pressure (SLP) anomalies for the region of 40–70°S. The NAO index is computed as the EOF of boreal winter (DJF) SLP anomalies in the North Atlantic area (90ºW-40ºE, 20º-70ºN).

We estimate the probability of no Granger causality by applying a test of Granger causality (Le and Bae, 2020; Mosedale et al., 2006; Stern and Kaufmann, 2013) for the multivariate predictive model shown in equation 1. For computing the degree of uncertainty, we followed recent guidance (Stocker et al., 2013) and utilized the terms ‘very unlikely’, ‘unlikely’, ‘likely’ for the 0–10%, 0–33%, and 66–100% probability of the likelihood of the outcome, respectively. For example, if the *p*-value is less than 0.33, the result indicates that ENSO is unlikely to display no Granger causality on ozone concentration. In this instance, we conclude that ENSO has ‘causal effect’ on ozone concentration.

References

Cai, W., Sullivan, A. and Cowan, T.: Interactions of ENSO, the IOD, and the SAM in CMIP3 Models, J. Clim., 24(6), 1688–1704, doi:10.1175/2010JCLI3744.1, 2011.

Hurrell, J. W., Kushnir, Y., Ottersen, G. and Visbeck, M.: An overview of the North Atlantic Oscillation, in Geophysical Monograph American Geophysical Union, pp. 1–35, American Geophysical Union., 2003.

Le, T. and Bae, D.-H.: Response of global evaporation to major climate modes in historical and future Coupled Model Intercomparison Project Phase 5 simulations, Hydrol. Earth Syst. Sci., 24(3), 1131–1143, doi:10.5194/hess-24-1131-2020, 2020.

Mosedale, T. J., Stephenson, D. B., Collins, M. and Mills, T. C.: Granger Causality of Coupled Climate Processes: Ocean Feedback on the North Atlantic Oscillation, J. Clim., 19(7), 1182–1194, doi:10.1175/JCLI3653.1, 2006.

Saji, N. H., Goswami, B. N., Vinayachandran, P. N. and Yamagata, T.: A dipole mode in the tropical Indian Ocean, Nature, 401(6751), 360–363, doi:10.1038/43854, 1999.

Stern, D. I. and Kaufmann, R. K.: Anthropogenic and natural causes of climate change, Clim. Change, 122(1–2), 257–269, doi:10.1007/s10584-013-1007-x, 2013.

Stocker, T. F., Qin, D., Plattner, G.-K., Alexander, L. V., Allen, S. K., Bindoff, N. L., Bréon, F.-M., Church, J. A., Cubasch, U., Emori, S., Forster, P., Friedlingstein, P., Gillett, N., Gregory, J. M., Hartmann, D. L., Jansen, E., Kirtman, B., Knutti, R., Kumar, K. K., Lemke, P., Marotzke, J., Masson-Delmotte, V. Meehl, G. A., Mokhov, I. I., Piao, S., Ramaswamy, V., Randall, D., Rhein, M., Rojas, M., Sabine, C., Shindell, D., Talley, L. D., Vaughan, D. G. and Xie, S.-P.: Technical Summary, in Climate Change 2013 - The Physical Science Basis, edited by Intergovernmental Panel on Climate Change, pp. 31–116, Cambridge University Press, Cambridge., 2013.

Table S1. List of CMIP6 models used in this study.

No.	Model name	Modelling center, country	Atmospheric Chemistry model
1	BCC_CSM2_MR	BCC, China	None
2	BCC_ESM1	BCC, China	BCC-AGCM3-Chem
3	CESM2	NCAR, United States	MAM4
4	CESM2_FV2	NCAR, United States	MAM4
5	CESM2_WACCM	NCAR, United States	MAM4
6	CESM2_WACCM_FV2	NCAR, United States	MAM4
7	CNRM_CM6_1	CNRM-CERFACS, France	OZL_v2
8	CNRM_CM6_1_HR	CNRM-CERFACS, France	OZL_v2
9	CNRM_ESM2_1	CNRM-CERFACS, France	REPROBUS-C_v2
10	IPSL_CM6A_LR	IPSL, France	None
11	MPI_ESM_1_2_HAM	MPI-M, Germany	Sulfur chemistry (unnamed)
12	MPI_ESM1_2_LR	MPI-M, Germany	None

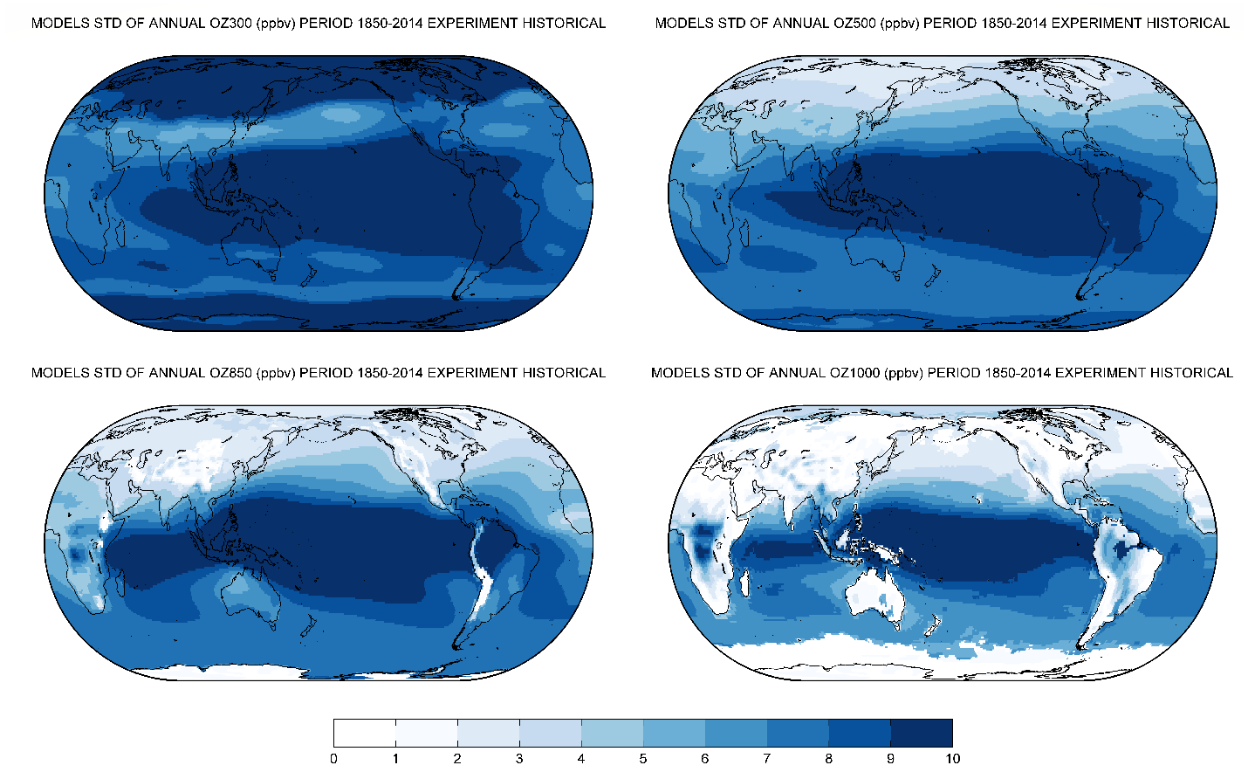

Figure S1. Multi-model mean map of standard deviation of annual ozone concentrations (ppbv) for the historical experiment over the 1850-2014 period at 300 hPa (a), 500 hPa (b), 850 hPa (c) and 1000 hPa (d) pressure levels, respectively.

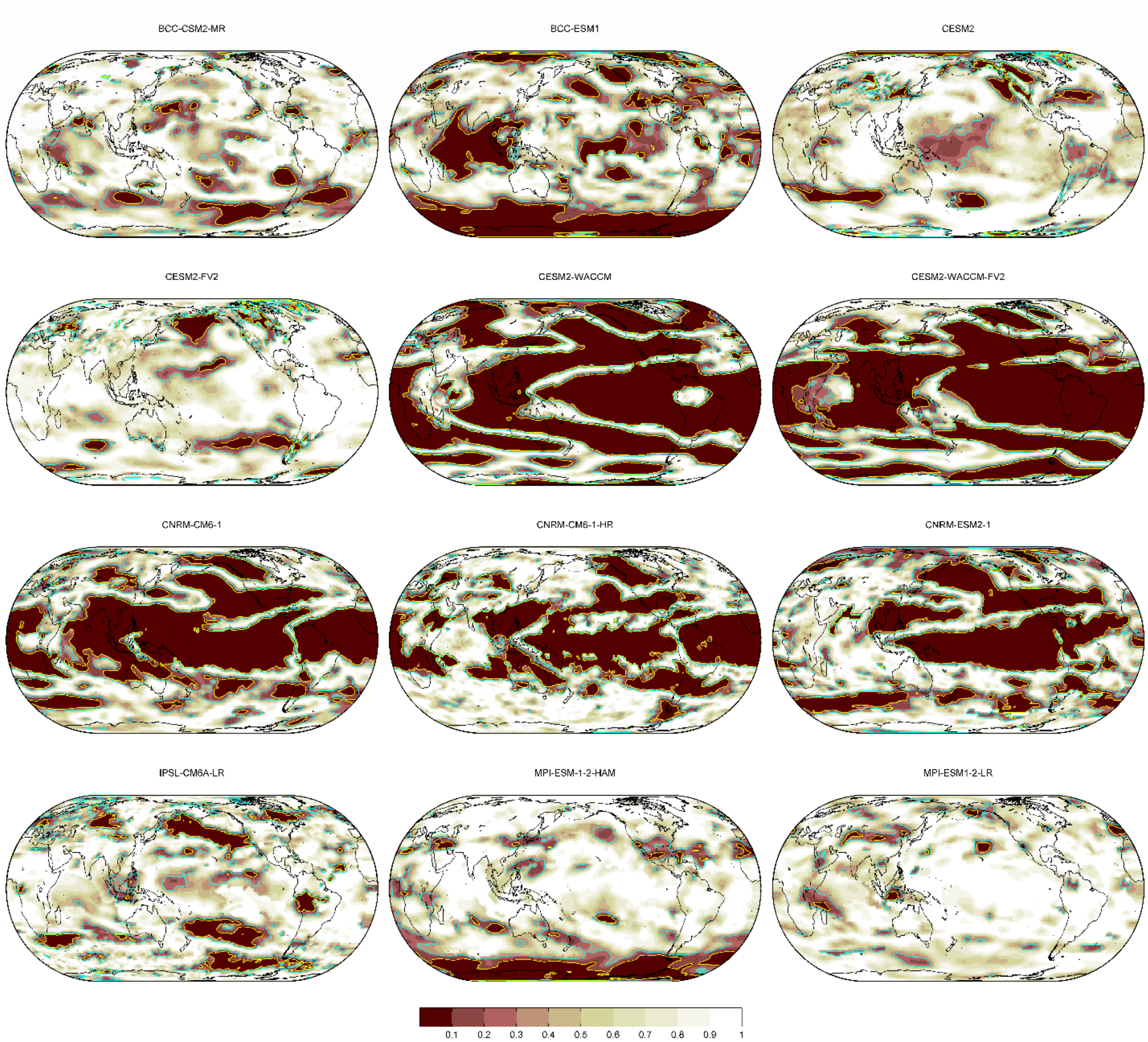

Figure S2. Probability for the absence of Granger causality from ENSO to annual ozone concentrations at 300 hPa pressure level for the historical experiment over the 1850-2014 period of 12 individual models (see Table S1). The cyan and yellow contour lines signify *p*-value = 0.33 and 0.1, respectively. Brown shades denote a low probability for the absence of Granger causality. ENSO: El Niño–Southern Oscillation.

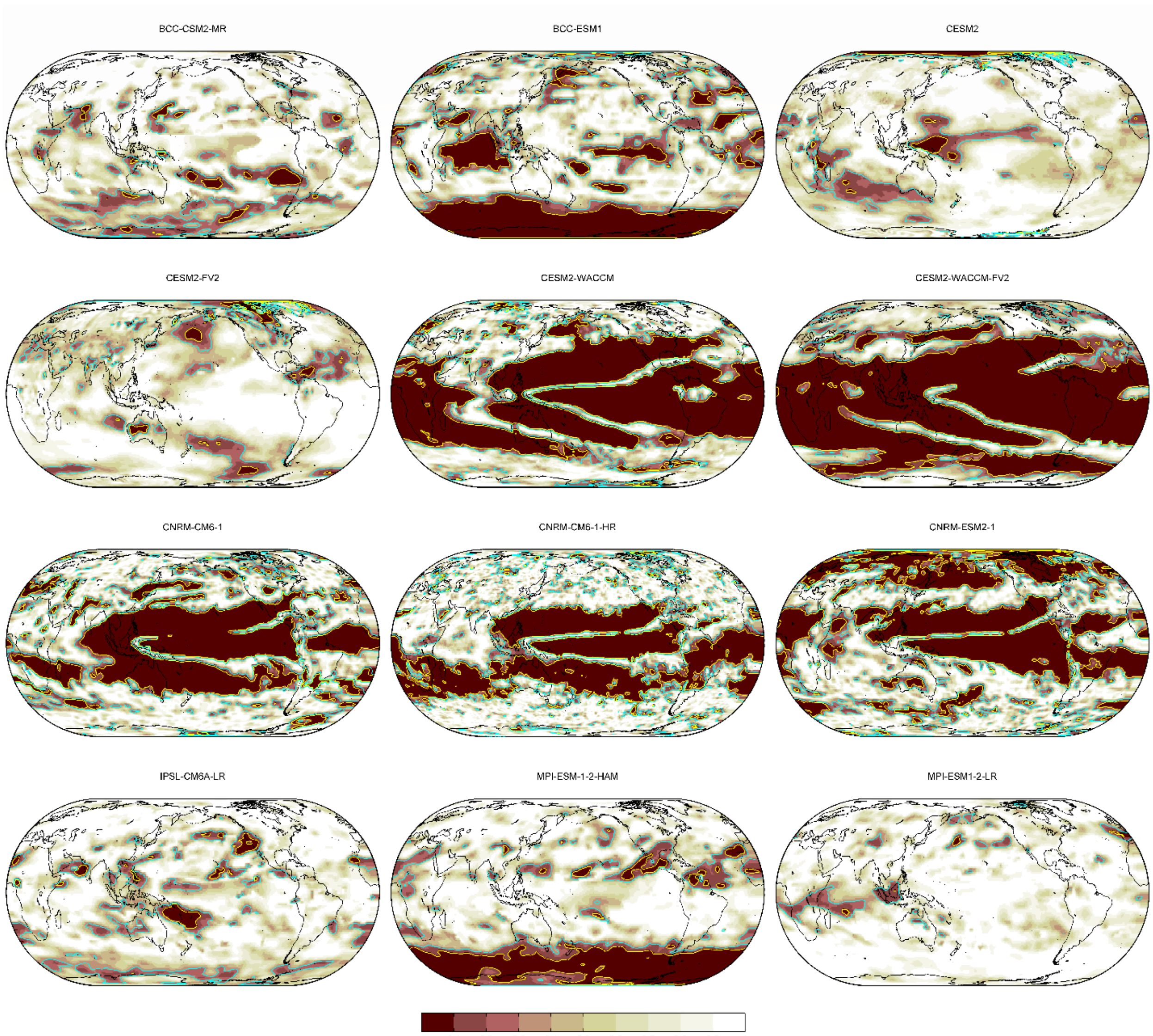

Figure S3. As in Figure S2, but for the absence of Granger causality from ENSO to annual ozone concentrations at 500 hPa pressure level. ENSO: El Niño–Southern Oscillation.

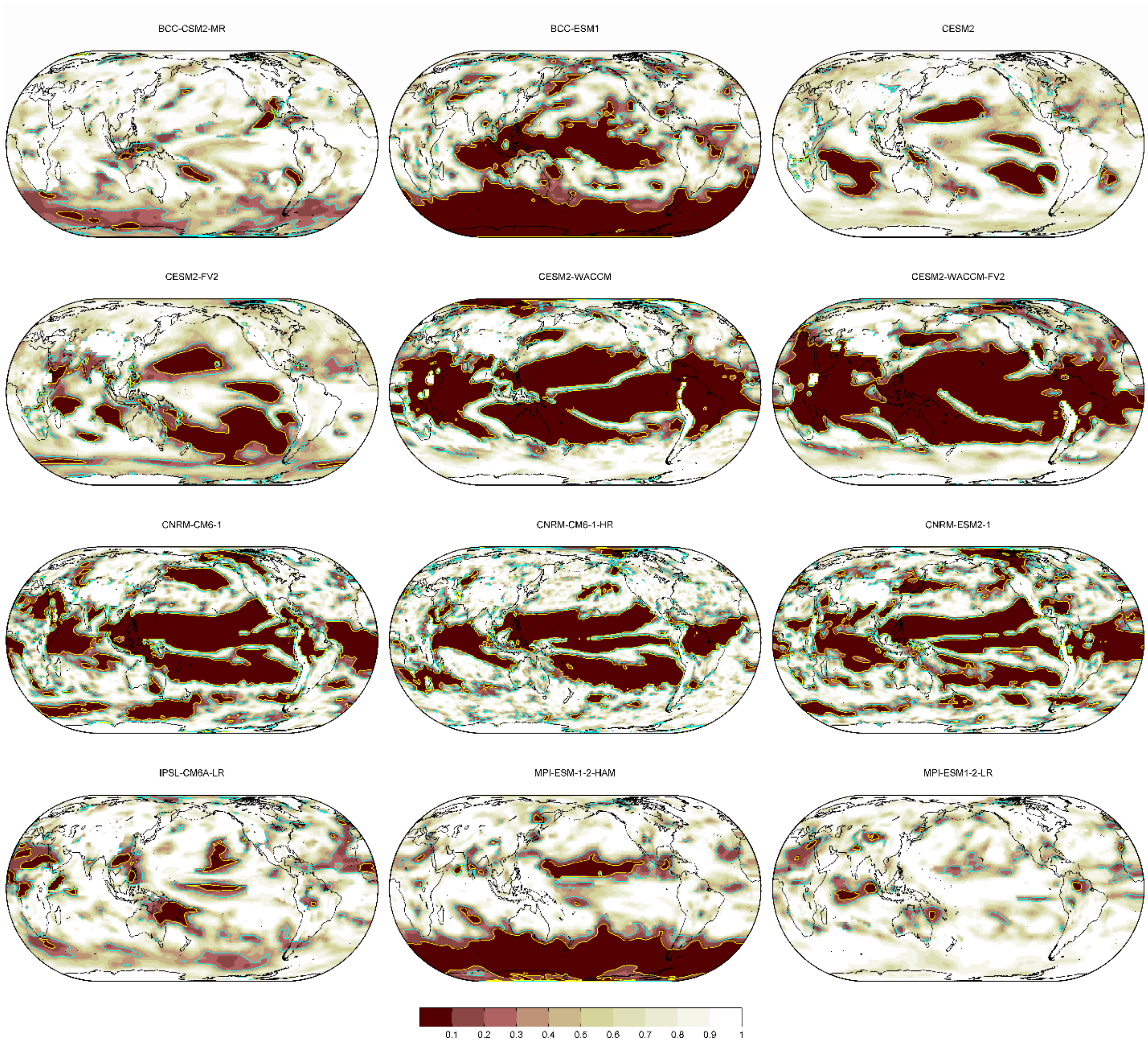

Figure S4. As in Figure S2, but for the absence of Granger causality from ENSO to annual ozone concentrations at 850 hPa pressure level. ENSO: El Niño–Southern Oscillation.

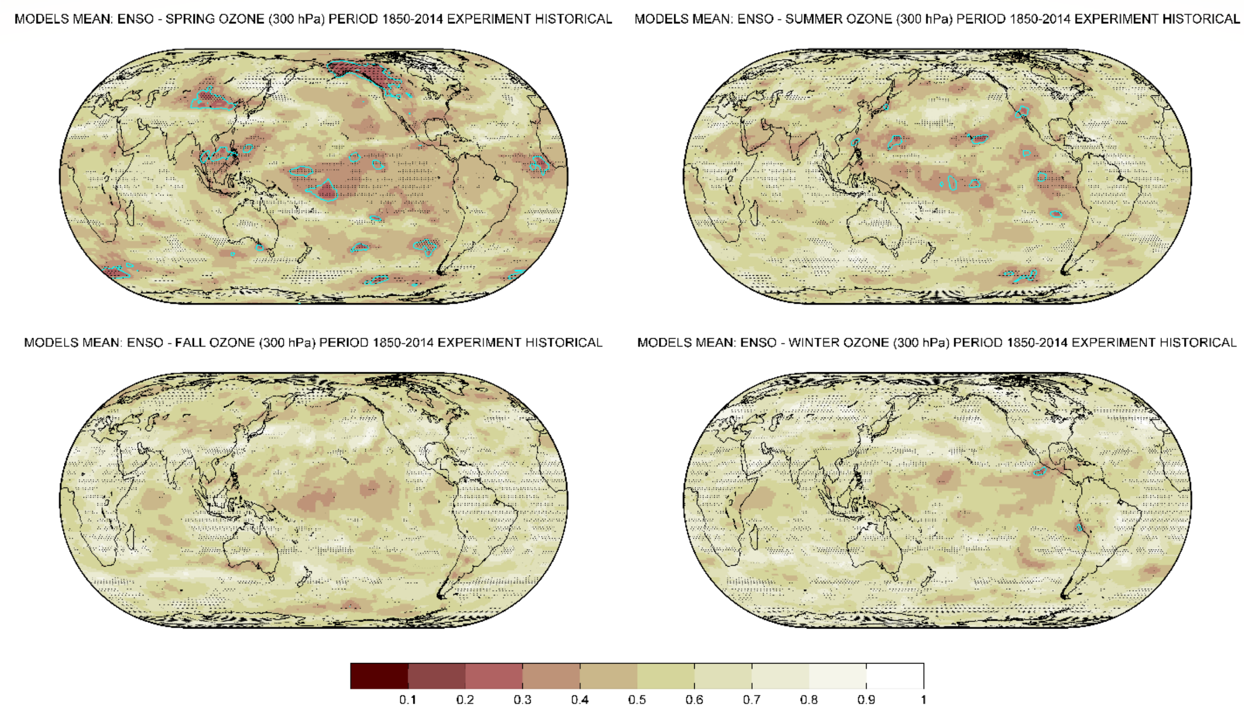

Figure S5. Multi-model mean probability map for the absence of Granger causality from ENSO during boreal winter [defined as D(*t*)JF(*t+1*); *t* denotes year *t*] to seasonal mean ozone concentrations at 300 hPa pressure level over the period 1850-2014. (a) Spring [March, April, May; MAM(*t+1*)]. (b) Summer [June, July, August; JJA(*t+1*)]. (c) Fall [September, October, November; SON(*t+1*)]. (d) Winter [December, January, February; D(*t+1*)JF(*t+2*)]. Stippling demonstrates that at least 70% of total models show agreement on the mean probability of all models at a given grid point. The cyan contour line signifies *p*-value = 0.33. Brown shades denote a low probability for the absence of Granger causality. ENSO: El Niño–Southern Oscillation.

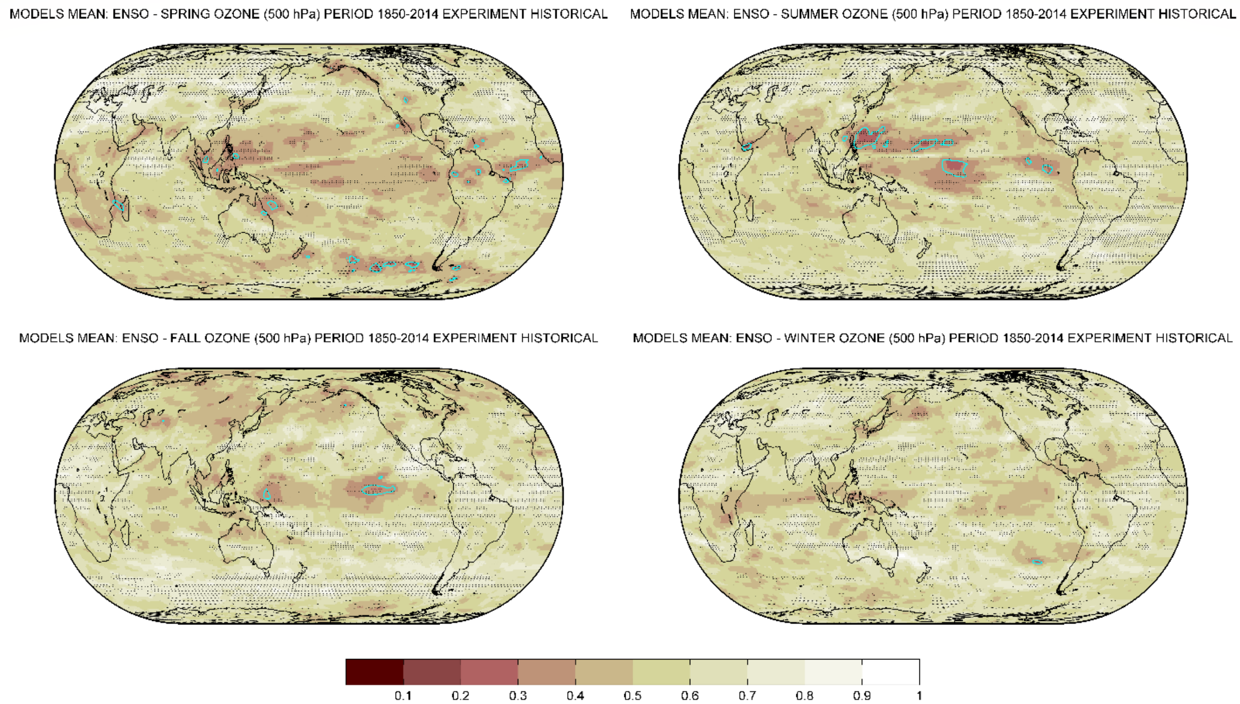

Figure S6. As in Figure S5, but for multi-model mean probability map for the absence of Granger causality from ENSO to seasonal mean ozone concentrations at 500 hPa pressure level. ENSO: El Niño–Southern Oscillation.

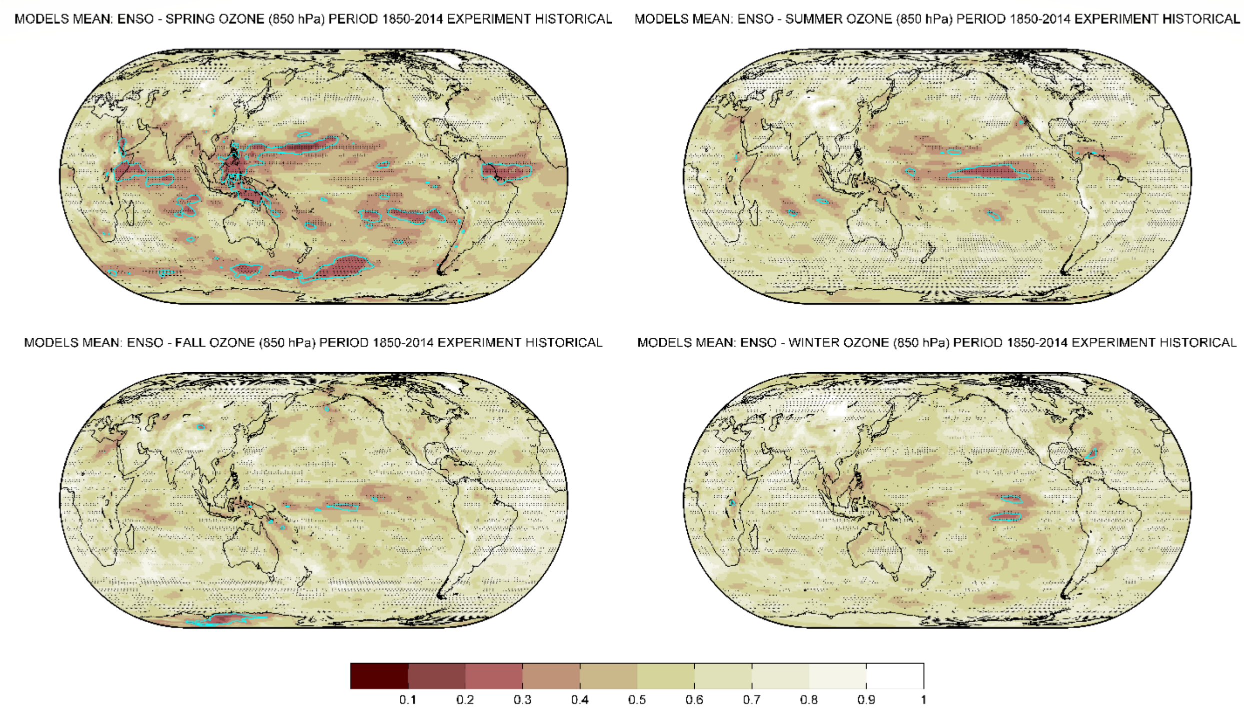

Figure S7. As in Figure S5, but for multi-model mean probability map for the absence of Granger causality from ENSO to seasonal mean ozone concentrations at 850 hPa pressure level. ENSO: El Niño–Southern Oscillation.